Microelectronic Engineering 129 (2014) 58–64

Contents lists available at ScienceDirect

Microelectronic Engineering

journal homepage: www.elsevier.com/locate/mee

On the fabrication and mechanism of pinecone surface structures

Qianqing Jiang [a], Wuxia Li [a,*], Jiajia Mu [a], Wangning Sun [a], Changzhi Gu [a,*]

[a] *Beijing National Lab of Condensed Matter Physics, Institute of Physics, Chinese Academy of Sciences, Beijing 100190, China*

ARTICLE INFO

Article history:
Received 12 May 2014
Accepted 12 July 2014
Available online 22 July 2014

Keywords:
3D metallization
Pinecone structures
Nanocones
Shadow effect

ABSTRACT

Nanostructured metal surfaces, in contrast to their corresponding bulk counterparts, have increased area, redistributed surface potential energy and novel physicochemical properties, thus have great potentials to be applied in a wide range of fields. In the work, different fabrication methods were employed to produce semiconducting and polymer conic structures, to provide three-dimensional frameworks with different surface properties, e.g. morphology, microstructure and chemical composition. Followed by metal deposition, 3D metalized conic structures, e.g. Ag–Si, Au/Ni–Si, Au/Ti–Si and Au/Cr–Si pinecones, were formed. The influence of factors, including the thickness and material type of the deposited metals, the metal deposition method, and the geometry, size and material type of the conic frameworks, on the 3D surface metallization process, were investigated and the related mechanisms were discussed.

1. Introduction

In surface sciences, it is well-known that it is the pre-structured surface of the substrate that has large affection on the related physical and chemical processes taken on it. Structured surfaces have increased area, redistributed surface potential energy and novel physicochemical properties, therefore, have great potential to be applied in many specific conditions [1–3]. Among various surface structures, cone-shaped structures have many unique properties, including large aspect ratio, small tip radius of curvature, high emission current density, superior electrical/thermal conductivity, robust mechanical strength, and good chemical stability [4,5]. It has been demonstrated that such structures have abundant functionalities in a broad range of application fields, e.g. near field optics [6,7], molecular detection by enhanced Raman scattering [8], and metamaterial [9].

Therefore, different methods have been developed by researchers to fabricate single or large area of conic surface structures and the related mechanisms have been proposed [10–18]. Zhang et al. reported the fabrication of ordered Si cone arrays with controllable morphologies and wettability by reactive ion etching system with two-dimensional silica colloidal crystals as masks [10]. Xu et al. reported the fabrication of self-organized vertically aligned single-crystal Si nanostructures with controlled shape and aspect ratio by reactive plasma etching [15]. Seo et al. reported a strategy of combined methods by electrochemical and chemical etching, though which precisely controlled vertical arrays of Si wires and cones have been fabricated [11]. In addition, direct laser writing (DLW), a technique that based on two-photon polymerization (2PP), has been widely used for the realization of arbitrary three-dimensional (3D) micro-/nanostructures [12–14]. However, issues such as how to effectively metalize the structured 3D surface in a controllable method and what the possible mechanisms would be related are required to be addressed.

In this work, we investigated the evolution of the 3D surface morphology during metal deposition on pre-fabricated conic structure. In particular, firstly, Si cones were fabricated in a reactive-ion etching-inductively-coupled-plasma (RIE-ICP) system. Then thin layers of metal were deposited to form Ag–Si, Au/Ni–Si, Au/Ti–Si and Au/Cr–Si surface structures via vacuum evaporation. It was found that for Si cones fabricated by RIE-ICP, the metal deposition resulted surface metallization obeys the mechanism of island growth; on the other hand, for FIB processed Si, diamond cones and IP-L polymer cones, island and layer by layer mixed growth have been observed. In more details, a completely formation of a pinecone structure could be characterized with four stages, namely, the initial metal atom seeding, the particle aggregation/nucleation, the steady shadowing 3D growth and the stacking pile-up growth. Systematic experiments were conducted to explore the trends and mechanism on metallization of 3D surfaces. Our results demonstrate that 3D structure fabrication followed by thin metal film deposition is an effective method for fabrication of metallic 3D surface structures; it potentially can be used to construct 3D devices, especially for SERs [6,7,9] and biosensors [8] due to the large surface area and possible improved surface plasmonic properties at the 3D interfaces [9].

* Corresponding authors.
E-mail addresses: liwuxia@aphy.iphy.ac.cn (W. Li), czgu@aphy.iphy.ac.cn (C. Gu).

http://dx.doi.org/10.1016/j.mee.2014.07.013
0167-9317/

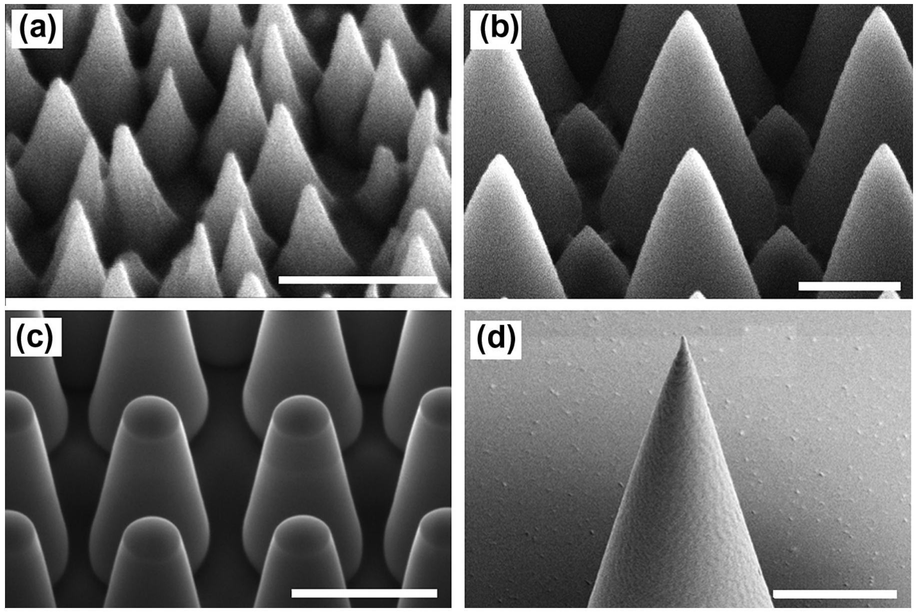

Fig. 1. Scanning electron microscope (SEM) images of arrays of: (a) random Si cones; (b) ordered Si cones; (c) ordered diamond cones; and (d) IP-L cones. The scale bar is 1 μm for (a–c) and it is 10 μm for (d).

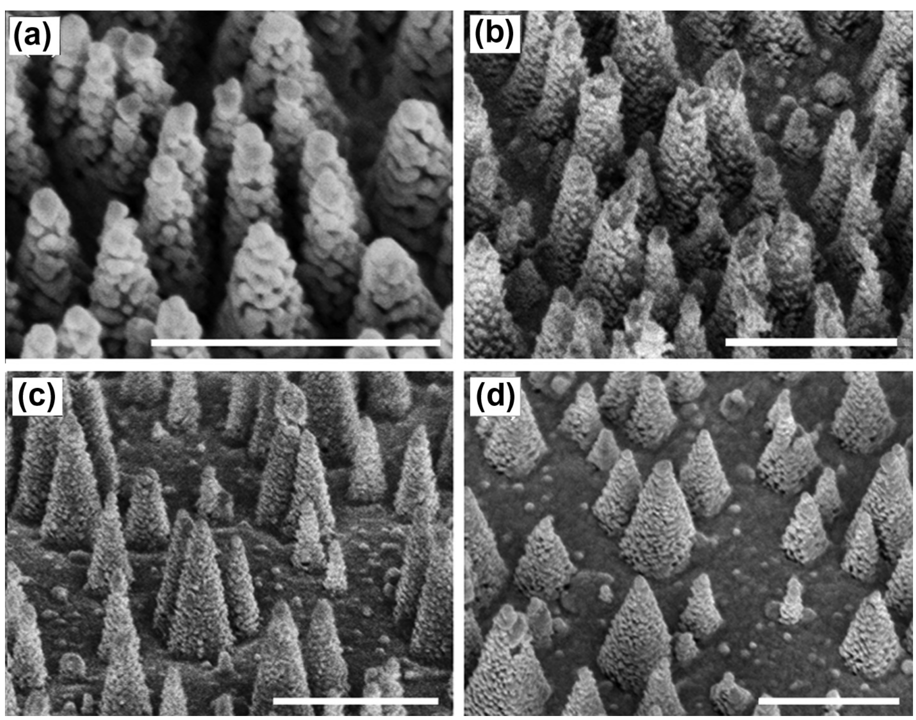

Fig. 2. SEM images of random distributed metal/Si pinecone structures with thermal evaporation of metal layers of: (a) Ag (70 nm); (b) Ni (5 nm)/Au (100 nm); (c) Ti (10 nm)/Au (80 nm); and (d) Cr (20 nm)/Au (100 nm). The scale bar is 500 nm.

2. Experimental

In this work, Si, diamond and IP-L cones were fabricated to serve as the pre-patterned 3D frameworks for 3D metallic surface structure fabrication. Silicon cones were obtained through a maskless etching with a reactive-ion etching-inductively-coupled-plasma (RIE-ICP) system. The reactive gas used was a mixture of O_2 and SF_6. After 7 min dry etching at −120 °C, large area of Si cones were obtained. The addition of O_2 was to form localized micro-/nano SiO_2 on the Si substrate, which could further serve as masks for Si etching. Mechanism of such self-organization process has been reported previously [17]. Diamond and Si cone arrays that with designable size, shape and distribution were fabricated through a commercially available SEM/FIB system utilizing a beam of 30 keV singly charged Ga^+ ions. During focused-ion milling, the base pressure was 2.4×10^{-6} mbar. The system was equipped with an advanced pattern generator (NanoBuilder), which offers flexibility for controlling the geometry, size, and distribution of patterns, potentially could be used to fabricate micro-/nano structure in sufficiently large area. For instance, to produce Si nanocones with density of $2.5 \times 10^5\ cm^{-2}$ in $1\ mm^2$ area, approximately 3 h is required. The system can hold sample with size up to 4 inches and it can be run overnight automatically. The ion beam is at an angle of 52° to the vertical, so the stage may be oriented with the ion beam perpendicular to the substrate surface for normal incident milling and SEM can be used for quality in-situ imaging. The polymer cone structures were fabricated by a commercial direct laser writing (DLW) system (Photonic Professional, *Nanoscribe GmbH*), which is based on two-photon polymerization (2PP) technology. In fabrication, a 780 nm femtosecond laser beam (with pulse width ~120 fs and repetition rate ~80 MHz) was focused into a negative photo-resist (IP-L, supplied by *Nanoscribe GmbH*) by a high numerical aperture (NA) oil-immersion objective (100X, NA 1.4, *Zeiss*).

Metal depositions were conducted by means of thermal evaporation under vacuum ($<10^{-4}$Pa), magnetron sputtering and electron beam evaporation with the film thickness and deposition rate monitored with a Quartz Monitor Crystals. Ti, Ni and Cr were deposited at a rate of 0.03 nm/s to serve as the adhesion layers, while the main surface metal layers, Ag and Au were deposited at a rate of 0.05 nm/s. Scanning electron microscopy was employed to examine the size and surface morphology of the metalized 3D surfaces.

3. Results and discussions

3.1. Fabrication of conic template structures

Four types of conic structures were used to investigate the trends and mechanism of 3D surface metallization. Fig. 1 shows the scanning electron microscope (SEM) images of typical random Si, ordered Si, diamond and IP-L conic structures. The cones shown in Fig. 1(a) were fabricated with a mixture of O_2 and SF_6 (40:18 sccm), the chamber pressure was 25 mTorr, the incident power was 1000 W and 4 W for ICP and RIE processing, respectively, and the DC bias was 44–46 V during etching. The density, size and topography of the cones can be easily modified with tuning the etching parameters such as the gas pressure, the ratio of O_2/SF_6, the RIE power and the etching time. Different Si cone arrays were fabricated to investigate the effects of the metal thickness

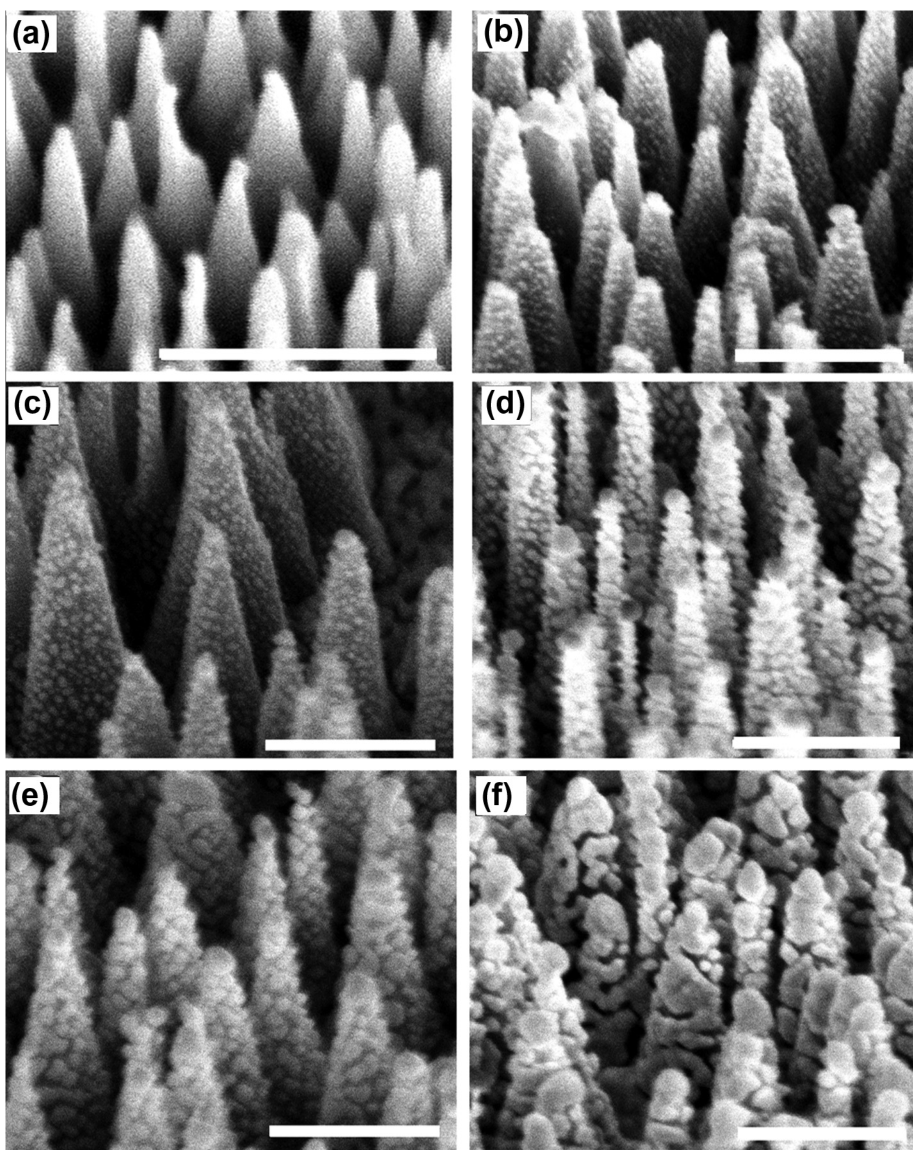

Fig. 3. SEM images of the as-formed Si cones (a) and those thermally evaporated with Ag layer of thickness of: (b) 8 nm; (c) 15 nm; (d) 30 nm; (e) 40 nm; and (f) 70 nm. The scale bar is 500 nm.

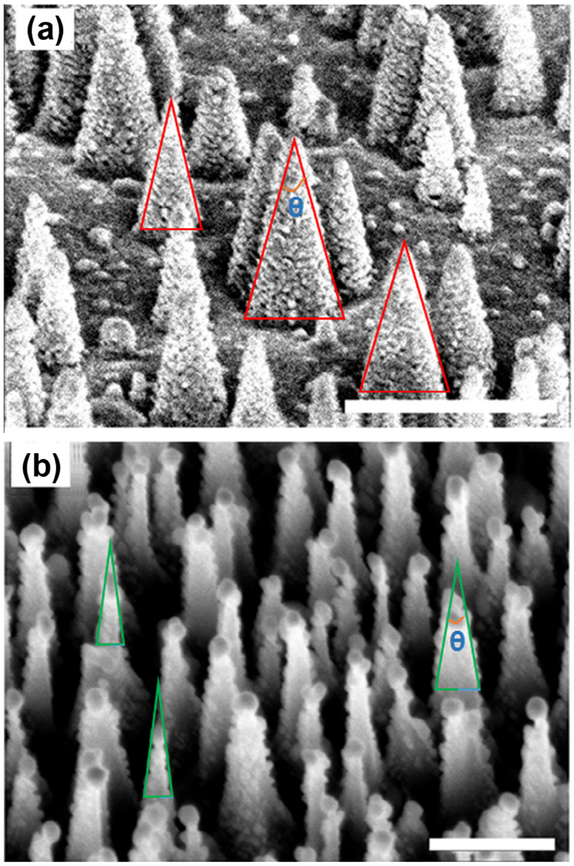

Fig. 4. SEM images of pinecone structures with different cone angle: (a) (20°–35°) with cone density of about 3.25×10^8 cones/cm^2; and (b) (10°–15°) with cone density about 6.51×10^8 cones/cm^2. The scale bar is 500 nm.

and the cone geometry on the 3D surface metallization process. Fig. 1(b) and (c) show highly orderly Si and diamond cone arrays, which were milled by focused-ion-beam with an ion beam current of 2.7 nA. By FIB direct writing, cones with desired shape, size and inter-distance can be fabricated site-specifically in a well-controllable way. Fig. 1(d) shows the IP-L polymer cone structure fabricated by laser direct writing. It can be seen that the slope of the sidewalls of conic structures etched by RIE-ICP varies with larger values on the cone top; by contrast, structures shown in Fig. 1(b)–(d) have uniform slope and smoothness.

3.2. Fabrication of pinecone structures

First of all, different metal materials were deposited on RIE-ICP fabricated Si cones. Fig. 2(a–d) show the side view SEM images of the resulted Ag (70 nm)/Si, Au (100 nm)/Ni (5 nm)/Si, Au (80 nm) /Ti (10 nm)/Si, and Au (100 nm)/Cr (20 nm)/Si pinecone structures. The layers of Ag, Au/Ti, Au/Ni and Au/Cr were deposited by thermal evaporation. Although there are discernable difference in the shape and morphology, clearly, different metal materials can be used to form pinecone-structures on Si cones fabricated through RIE-ICP etching. It is worth noting that, although Fig. 2(a)–(d) shows that the surface morphology of each individual pinecone structures is not obviously dependent on the size and distribution of the Si cones, the morphology of the final surface might be closely related to the shape of the cone, as well as the thickness and material type of the deposited atoms. The effects of these factors will be discussed in more details in the following sections.

3.3. Metal-layer-thickness related evolution of the 3D surface morphology

Fig. 3(a)–(f) are the SEM images showing the morphological evolution of the Ag/Si 3D nanostructures formed at various deposition stages corresponding to different Ag thicknesses. It can be seen that increasing of the deposition time resulted in apparent morphology changes. In the initial stage as shown in Fig. 3(b), when the deposited Ag thickness is 8 nm, Ag particles with average grain size of about 13 nm (measured from higher magnification SEM image that not shown here) can be seen evenly deposited onto the sidewall of the cones. Fig. 3(c) shows uniform grain growth with increasing the thickness. Whereas, it is remarkable to note that when the deposited metal thickness reached 30 nm, pinecone structure gradually formed on the upper part of the cone; but in

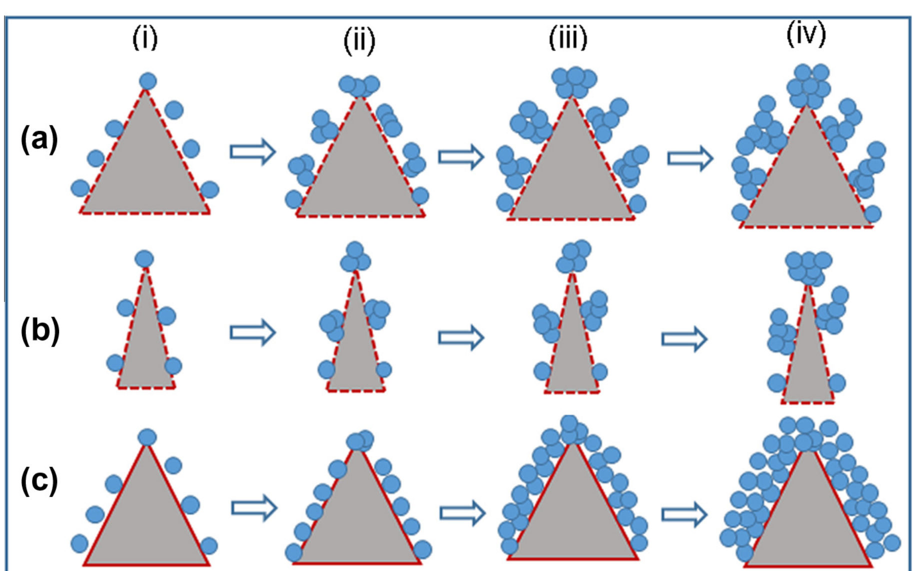

Fig. 5. Ag film thickness and Si cone angle (fabricated by RIE-ICP) dependent particle size distribution: (a) 15 nm Ag on Si cones with cone angle of 20°; (b) 40 nm Ag on Si cones with cone angle of 20°; (c) 40 nm Ag on Si cone with cone angle of 35°.

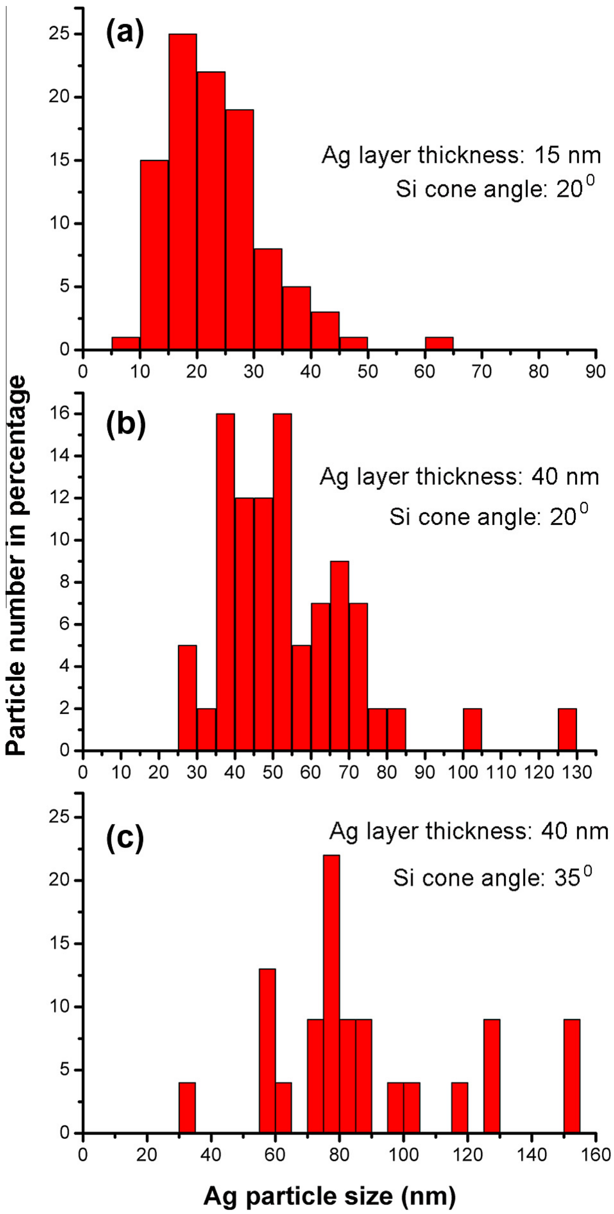

Fig. 6. The schematics showing the process of surface morphology evolution on different cone structures: (a) and (b), formation of pinecone structures surface with poor metal wettability; and (c) formation of continuous 3D surface on cone with good metal wettability.

the lower part, small Ag particles still can be seen (Fig. 3(d)). By increasing the Ag thickness up to 40 nm, a more complete pinecone-structure was obtained as shown in Fig. 3(e). Further increasing the Ag thickness up to 70 nm, Ag patches were found stacked out with clear gaps between each other and finally joint together. Thus, the growth could be divided into four stages, namely, the initial metal atom seeding, the metal atoms aggregation/nucleation, the steady shadowing growth and the stacking pile-up growth. Meanwhile, in the case of using Au as the surface layer, a same trend was observed but the pinecone structures have smaller overall volume compared with the Ag pinecone structures. We also found that planar Au films on unstructured Si were denser than Ag films when a same thickness was deposited with a same deposition rate, possibly due to the higher surface energy of the deposited Au atoms compared to that of Ag atoms.

In addition, it can be seen that the evaporated atoms preferred to gather at the top end of the cones. As the deposition continued, the flakes continued to grow with those at the upper side had the maximized growth rate, turns the top tips to be ball-shaped.

3.4. The effects of the cone geometry

In order to elucidate the influence of the size and shape of the conic structures on 3D surface metallization, Si cones with various sizes and aspect ratios were fabricated followed by Ti (10 nm)/Au (80 nm) deposition. Fig. 4(a) and (b) show the surface morphology of cones after metal deposition, which have cone angle (θ) in the range of (20–35°) and (10–15°), respectively. It can be seen from Fig. 4(a) that complete pinecone structures with uniform flakes were obtained. However, for cones that with smaller cone angles as shown in Fig. 4(b), the lower parts of the cones were sheltered by the top parts, with balls of size comparable to the cone bases were formed, preventing the evaporated atoms to be transported to the lower parts.

Moreover, Ag with thicknesses of 15 nm, 30 nm and 70 nm were deposited on RIE-ICP fabricated cones with different cone angles. For Ag film of 30 nm and 70 nm, similar trends were observed as those using Ti (10 nm)/Au (80 nm). For more details, particle size distribution was derived for comparison. For irregular particles, the size was characterized by the largest dimension. Selected values are shown in Fig. 5. It can be seen that for the 15 nm Ag deposited conic surfaces, most of the particles were about 10–30 nm in size and they are more uniformly distributed when compared with those on the 40 nm Ag deposited cones. Clearly, larger particles grew faster with increasing of the deposited metal thickness, and the size distribution tended to be more dispersed. Comparison between Fig. 5(b) and (c), one can see that

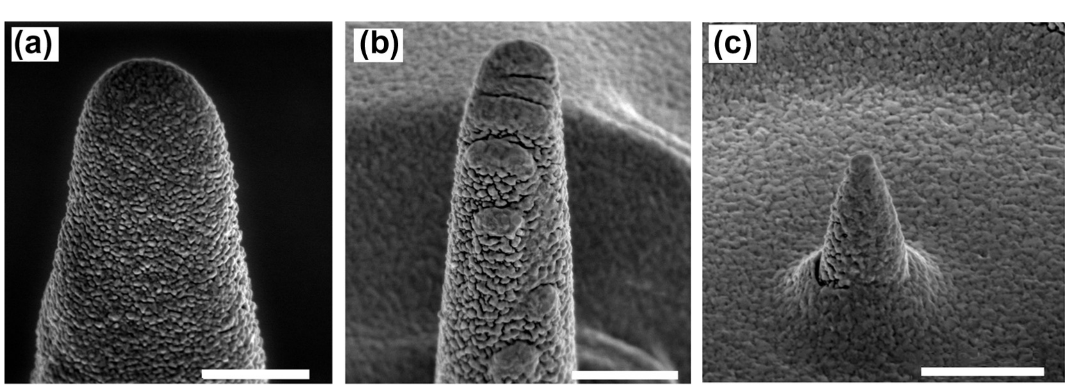

Fig. 7. The influence of the cone material on 3D surface metallization: (a) IP-L; (b) FIB processed polycrystalline diamond and (c) FIB processed Si cones. The metals are thermally evaporated Cr (5 nm) and Au (70 nm). The scale bar is 500 nm.

larger cone angle could result in larger grain size with wider size distribution. These observations confirm that the cone angle (can be divided into several regions with critical values) and the film thicknesses are main factors that affect the final morphology of the 3D surfaces.

3.5. Mechanism of the 3D surface metallization

Growth of metal atoms on planar substrates can be classified into three different mechanisms: (i) island growth mode, in that the interfacial energy together with the film surface energy exceeds the substrate surface energy, atoms have very slow diffusion on the substrate and are more strongly bound to each other than to the substrate, thus deposited atoms tend to form three dimensional islands; (ii) layer by layer growth mode, a case that substrate generally has highest crystalline quality, and the deposited atoms are more strongly bound to substrate than to each other with fast diffusion on the substrate; (iii) mixed growth of the former two, in this case, initially, the growth is layer by layer and then by island to form three dimensional islands. Such behaviors have been observed in epitaxial growth of metal films and related mechanisms have been proposed [19–23].

Obviously, on flat substrates, islands growth gives rise to rough film surface. And it is not hard to imagine that on conic structured surfaces, when the islands reach a certain size, the formation of 3D islands could lead to a new effect – shadowing. For detailed description, we characterized the 3D surface metallization process with four distinct steps. Fig. 6(a) and (b) illustrate the process for 3D surfaces that have poor/anisotropy metal wettabilities. In the initial stage, the deposited atoms are landed uniformly on the substrate (step (i)). These atoms then tend to coalesce into individual isolated islands (step (ii)) to minimize the surface free energy, as can be evident from the clearly seen particles in Fig. 3(b) when a nominal film thickness of 8 nm was deposited. As the deposition continues, the growth turns to step (iii) with islands grow in all three dimensions but preferred vertically. Thus, the isolated particles start to coalesce with atoms pile up one on top of the other. Consequently, the fast vertical growth results in blocking of the forthcoming atoms from landing on the areas beneath. Since the forthcoming atoms tend to adhere to the topsides of the metal islands, nano protuberances were formed to cause shadowing effect, a phenomenon that is absent in planar film growth. Finally, with increasing the evaporation time, metal atoms piled up to form compound structures resemble a pinecone as shown in Fig. 3. With deposition further continues, the upper parts of each pinecone flakes enlarged and quasi-continuous metal surface are obtained as shown in step (iv) in Fig. 6(a). For cones with smaller conic angles as shown in Fig. 6(b), the shadowing effect is more significant and the efficient surface area for receiving the evaporated atoms could be greatly reduced by the top part of the cone.

However, for cones with good/isotropic surface wettability, and small conic angles as shown in Fig. 6(c), the surface morphology evolution might be different from those presented in Fig. 6(a) and (b), but similar to that of a planar surface. To verify such assumption, FIB processed diamond cones and polymer IP-L cones were used as the 3D frameworks. As shown in Fig. 7, different from

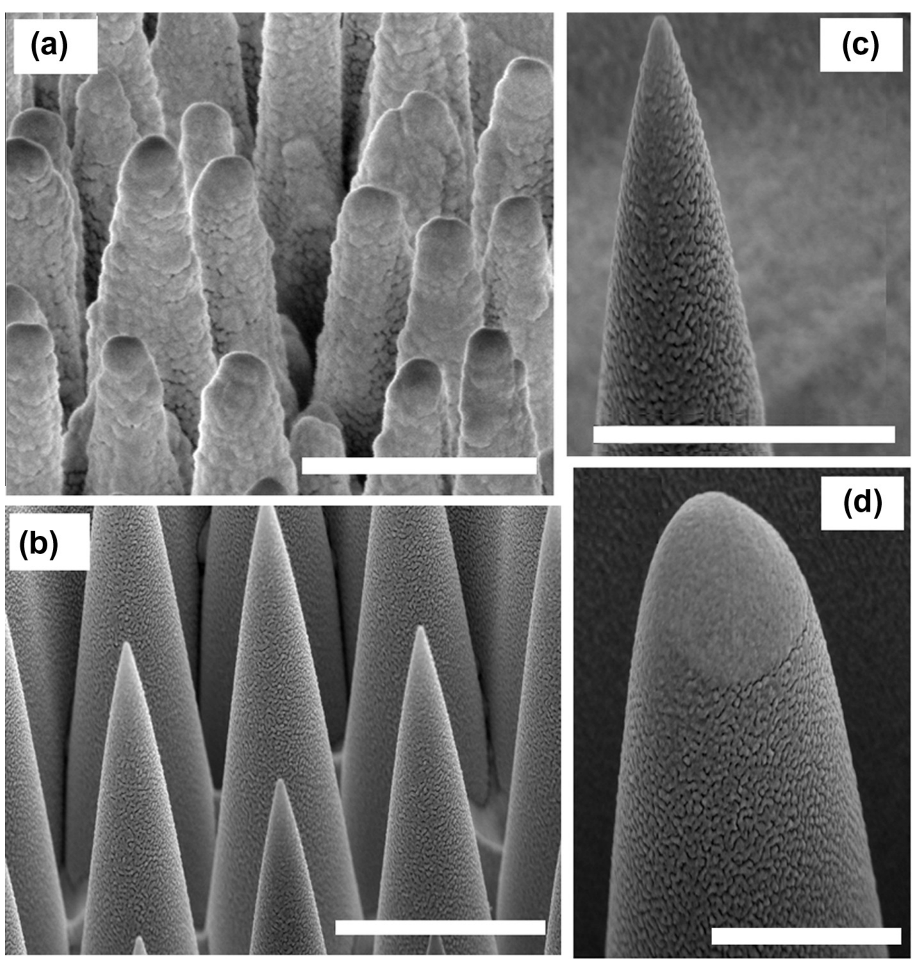

Fig. 8. The influence of the metal deposition methods on the morphology of 3D surface metallization: (a) magnetron sputtered 30 nm Au on RIE-ICP etched Si cones; (b–d) electron beam evaporation of Au (30 nm)/Cr (3 nm) on FIB processed Si cones. The scale bar is 500 nm for (a), 2 μm for (b), 1 μm for (c) and (d).

those on Si cones processed by RIE-ICP, grainy surface rather than pinecone structures was found and there is no obvious different in the morphology between the substrate and the sidewall of the cones, even when the thickness of the deposited films reached 75 nm. This may attribute to the amorphous nature of the uttermost surface layers of such cones, with which the deposited metal atoms were evenly absorbed without cluster gathering at the initial stage, therefore, shadowing effect is greatly reduced. These results clearly suggest that the geometry/microstructure of the supporting substrate, as well as the material type (alternatively, the surface energy of the supporting surface), are factors that determine the growth behavior of deposited atoms on 3D surfaces.

It is well-known that during metal deposition, when metal atom strikes the surface, it loses its energy and condenses on the surface. Upon the condensation, the atoms have some mobility on the surface depends on the surface energy, which are defined by their kinetic energy and the strength and types of interactions between the atoms, the clusters of atoms and the substrate surface. In general, materials with lower surface energy tend to stick less to other materials and reduced surface energy will lead to a weaker bond between these two phases, thus the deposited atoms are susceptible to form isolated islands. The FIB etched Si and diamond cones have been reported to have an amorphous layer with thickness of a few tens of nm due to Ga^+ bombardment. According to the Frank–van der Merwe growth mechanism, atoms on such amorphous surface are intended to be trapped in each particular site and less keen to form isolated islands. In that, the shadowing effect could be completely excluded in the surface metallization, leading to formation of uniformly covered 3D surface. So is for the IP-L polymer cones. In addition, compared to Si cones formed by FIB, RIE-ICP etched cones have rougher sidewalls with possibly larger amount of tiny steps and kinks, and there is deviation of the sidewall slopes, which may provide more preferred sites for atom nucleation.

For comparison, Si cones were fabricated by FIB and Cr (5 nm)/Au (70 nm) were deposited on the surface by thermal evaporation, Fig. 7(c) shows the corresponding surface morphology. Different from those on RIE-ICP fabricated Si cones, continuous cone surface was formed. This is because FIB processing usually introduces additional Ga^+ into the irradiated material and causes amorpholization of the surface layer; while RIE and ICP with Ar plasma are widely used to remove the surface contamination/damages aroused during FIB processing. In that, the surface properties, including the morphology, micro-structure and chemical composition of FIB and RIE-ICP processed cones are different. In addition, the metallization behavior may also be affected by other conditions such as the choice of metal deposition method. For this purpose, Au was deposited by magnetron sputtering and electron beam evaporation. Fig. 8(a)–(d) shows the corresponding results that no pinecone was observed. Compared with thermal evaporation, magnetron sputtering and electron beam evaporation could provide released atoms with more energy, thus the growth behavior is more resemble the Stranski–Krastanov mode. These results further indicate that changes in the surface energy, either by the properties of the conic surface, or the deposition method, can lead to distinct metalized surface morphologies.

4. Conclusion

To sum up, we investigated the 3D metallization process and mechanism on various conic surfaces. In particular, the influence of the material type, the thickness and the deposition method of the surface metal layer, and the material, the shape and fabrication method of the supporting 3D surfaces, on the metallization process and 3D morphology evolution, were examined in details. Particles/islands initiation, particles/islands expansion, pinecone structure realization and coalescent of continuous 3D surface structure were proposed to describe the metallization process. We found that larger particles grew faster with increasing of the deposited metal thickness, thus lead to more obvious shadowing effect, which is the mechanism that responsible for the pinecone formation. Also, larger cone angle could result in larger grain size with wider size distribution. These observations confirm that for a particular metal deposition method, the geometry and the surface properties of the 3D framework as well as the film thicknesses are main factors that affect the final morphology of the metalized 3D surfaces. Although more in-depth experiment is required to characterize the surface energy, chemical composition and micro-structures on the effective contact area, the density of the deposited atoms and the metal crystalline orientation of the formed material system, nevertheless, we can change Si to other materials, and the cone-structured surface can be replaced by other geometries, together with proper deposition materials chosen, this pinecone-like structures may have potential applications in optics [24] and biochemistry [25].

Acknowledgments

This work is supported by the Technical Talent Program of the Chinese Academy of Sciences; the National Natural Science Foundation of China under Grants Nos. 91123004, 11104334, 51272278, 61390503, 91023041 and 91323304.

References

[1] B. Bhushan, Langmuir 28 (2012) 1698–1714.
[2] Y. Xiu, Y. Liu, D.W. Hess, C.P. Wong, Nanotechnology 21 (2010) 155705.
[3] M. Helfrich, R. Gröger, A. Förste, D. Litvinov, D. Gerthsen, T. Schimmel, D.M. Schaadt, Nanoscale Res. Lett. 6 (2011) 211.
[4] C.-F. Lin, C.-M. Lin, K.-T. Chen, J.-J. Dai, M.-S. Lin, IEEE Electron Dev. Lett. 31 (2010) 458.
[5] Z. Xiao, M.S. Sarwar, M. Dahmardeh, M.V. Moghaddam, A. Nojeh, K. Takahata, Appl. Phys. Lett. 103 (2013) 171603.
[6] M. Fleischer, W.B. Alexander, M.V.P. Altoe, A.M. Schwartzberg, P.J. Schuck, S. Cabrini, D.P. Kern, ACS Nano 5 (2011) 2570–2579.
[7] R. Kodiyath, T.A. Papadopoulos, J. Wang, Z.A. Combs, H. Li, R.J.C. Brown, J. Phys. Chem. C 116 (2012) 13917.
[8] N.C. Linn, Nanotechnology 20 (2009) 225303.
[9] F.D. Angelis, Z.R. Proietti, M. Francardi, C. Liberale, E.D. Fabrizio, Opt. Express 19 (2011) 22268.
[10] X. Zhang, J. Zhang, Z. Ren, X. Li, X. Zhang, D. Zhu, T. Wang, Langmuir 25 (2009) 7375.
[11] H.S. Seo, X. Li, H.-D. Um, B. Yoo, Mater. Lett. 63 (2009) 2567.
[12] S. Kawata, H.B. Sun, T. Tanaka, K. Takada, Nature 412 (2001) 697.
[13] B. Jia, J. Li, M. Gu, Aust. J. Chem. 60 (2007) 484.
[14] Z.S. Gan, Y.Y. Cao, R.A. Evans, M. Gu, Nat. Commun. 4 (2013) 3061.
[15] S. Xu, I. Levchenko, S.Y. Huang, K. Ostrikov, Appl. Phys. Lett. 95 (2009) 111505.
[16] E. Gogolides, V. Constantoudis, G. Kokkoris, D. Kontziampasis, K. Tsougeni, G. Boulousis, M. Vlachopoulou, A. Tserepi, J. Phys. D: Appl. Phys. 44 (2011) 174021.
[17] I. Levchenko, U. Cvelbar, K. Ostrikov, Appl. Phys. Lett. 95 (2009) 021502.
[18] K. Ostrikov, E.C. Neyts, M. Meyyappan, Adv. Phys. 62 (2013) 113.
[19] R. Koch, D. Hu, A.K. Das, Phys. Rev. Lett. 94 (2005) 146101.
[20] D.J. Eaglesham, M. Cerullo, Phys. Rev. Lett. 64 (1990) 1943.
[21] F.C. Frank, J.H. van der Merwe, Proc. R. Soc. London A 198 (1949) 205.
[22] M. Volmer, A. Weber, Z. Phys. Chem. 119 (1926) 277.
[23] I.N. Stranski, V.L. Krastanow, Akad. Wiss. Lit. Mainz Math.-Natur. Kl. IIb 146 (1939) 797.
[24] Kh. Nerkararyan, T. Abrahamyan, E. Janunts, R. Khachatryan, S. Harutyunyan, Phys. Lett. A 350 (2006) 147.
[25] Deng. Y-L, Biosens. Bioelectron. 53 (2014) 37.